




# Heavy quark potential and LQCD based quark condensate at finite magnetic field

Indrani Nilima<sup>1</sup>, Aritra Bandyopadhyay<sup>2,3</sup>, Ritesh Ghosh<sup>4,5,6,a</sup> , Sabyasachi Ghosh<sup>7</sup>

<sup>1</sup> Department of Physics, Banaras Hindu University, Varanasi 221005, India

<sup>2</sup> Guangdong Provincial Key Laboratory of Nuclear Science, Institute of Quantum Matter, South China Normal University, Guangzhou 510006, China

<sup>3</sup> Institut für Theoretische Physik, Universität Heidelberg, Philosophenweg 16, 69120 Heidelberg, Germany

<sup>4</sup> School of Physical Sciences, National Institute of Science Education and Research, HBNI, Jatni, Khurda 752050, India

<sup>5</sup> Theory Division, Saha Institute of Nuclear Physics, 1/AF, Bidhannagar, Kolkata 700064, India

<sup>6</sup> Homi Bhabha National Institute, Anushaktinagar, Mumbai, Maharashtra 400094, India

<sup>7</sup> Indian Institute of Technology Bhilai, GEC Campus, Sejbahar, Raipur, Chhattisgarh 492015, India

Received: 23 September 2022 / Accepted: 3 January 2023 / Published online: 17 January 2023

© The Author(s) 2023

**Abstract** In the present work, we have studied heavy quarkonia potential in hot and magnetized quark gluon plasma. Inverse magnetic catalysis (IMC) effect is incorporated within the system through the magnetic field modified Debye mass by modifying the effective quark masses. We have obtained the real and imaginary part of the heavy quark potential in this new scenario. After the evaluation of the binding energy and the decay width we comment about the dissociation temperatures of the heavy quarkonia in presence of magnetic field.

## 1 Introduction

A lot of information is being provided by the ongoing relativistic heavy-ion collisions (HIC) in respect of deconfined state of matter, i.e. quark gluon plasma (QGP). QGP at sufficiently high temperature behaves like a weakly interacting gas of quarks and gluons, which can also be studied perturbatively by using hard thermal loop (HTL) resummation [1–4] techniques, apart from the first principle lattice QCD estimations. Depending on the non-centrality, HIC can also produce a very strong magnetic field in the direction perpendicular to the reaction plane [5, 6]. At the RHIC energies, the estimated strength of the magnetic field is around  $B \sim m_\pi^2 \equiv 10^{18}$  Gauss whereas at the LHC the estimated strength is around  $B \sim 15m_\pi^2 \equiv 1.5 \times 10^{19}$  Gauss [5, 6], where  $m_\pi$  is the pion mass. The issue – whether this large initial magnetic

field will decay very fast [7] or slow [8, 9] is still probably an open problem. Studies have also shown that such an extensive magnetic field might even have survived from the very early stages of universe [10, 11]. These possibilities provide the opportunity to revisit the entire QGP phenomenology in presence of magnetic field, and in the present work we have attempted the same with heavy quark phenomenology.

According to recent lattice quantum chromodynamic (LQCD) calculation [12, 13], non-zero QCD vacuum at finite temperature and magnetic field can face both magnetic catalysis (MC) and inverse magnetic catalysis (IMC). MC shows the low temperature enhancements in the values of quark condensates with increasing magnetic field and extensively studied through lattice QCD and effective models. On the other hand, IMC shows a decreasing behaviour of the condensates with increasing magnetic field close to the transition temperature. IMC was first discovered by lattice QCD simulations using physical values of pion mass and for the light quarks. Since then there have been many efforts to implement IMC in the effective models. In our present work, we have implemented this important IMC effect in our calculation through the constituent quark mass generated by the lattice QCD simulations, which incorporates the complex and non-monotonic temperature and magnetic field dependence within the quark condensates.

One of the useful probe of the QGP formation is heavy quarkonium which is a bound state of  $Q\bar{Q}$  pair [14, 15]. After the discovery of  $J/\psi$  (a bound state of  $c\bar{c}$ ) [16, 17], in 1974, a large number of excellent articles have been published that proposed several essential refinements in the study of heavy quark potential. The first work to study the

<sup>a</sup> e-mail: [riteshghosh1994@gmail.com](mailto:riteshghosh1994@gmail.com) (corresponding author)

quarkonia at finite temperatures using potential models have been done by Karsch, Mehr, and Satz [18]. Subsequently another pioneering work to study the dissociation of quarkonia due to the color screening in the deconfined medium with finite temperature, was carried out by Matsui and Satz [19]. In recent years various studies have been executed to see the impact of magnetic field on heavy quark phenomenology [20–36]. Specifically speaking, the effects of the external magnetic field on the quarkonia production have been discussed in Refs. [23,28]. In Ref. [32], the authors have studied the directed flow of charm quarks which is considered as an efficient probe to characterize the evolving magnetic field produced in ultra-relativistic HIC. In Ref. [29] the authors have investigated QCD sum rules in calculation of the mass of heavy mesons to estimate the modification of the charged B meson mass, ( $m_B$ ), in the presence of an external Abelian magnetic field. The momentum diffusion coefficients of heavy quarks, in a strong magnetic field within the lowest Landau level (LLL) approximation, along the directions parallel and perpendicular to  $B$ , at the leading order in QCD coupling constant have been computed within and beyond the static limit of the heavy quarks, respectively in Refs. [31] and [36].

The physics about the fate of quarkonia at zero temperature can be understood with the help of non-relativistic potential models. Masses of heavy quarks ( $m_Q$ ) are much larger than QCD scale ( $\Lambda_{QCD}$ ) and velocity of the quarks in the bound state is small,  $v \ll 1$  [37]. Hence, to understand the binding effects in quarkonia generally one uses the Cornell potential which belongs to the family of the non-relativistic potential models [38] and can be derived directly from QCD using the effective field theories (EFTs) [37–39]. Refs. [33,35] has studied the effect of a strong magnetic field on the heavy quark complex potential within the lowest Landau level (LLL) approximation. In this regard, present work has moved beyond LLL estimation and considered all Landau level summation, which is valid for the entire range of magnetic fields, from weak to strong. This is one of the new ingredients of the present work. The main goal of the present work though is to incorporate the IMC effect in the heavy quark potential through the effective quark masses. These two components are mainly introduced within the standard formalism of heavy quark potential [41,42,44,45,49], which is the sum of both Coulomb and string terms [40].

The paper is organized as follows. In Sect. 2, we will discuss the basic formalism of our present work which includes discussions about the real and imaginary parts of the heavy quark potential, decay width, binding energy and the Debye screening mass. In Sect. 3 we will show our results for the same as well as find out the dissociation temperatures and discuss their magnetic field dependence. Finally in Sect. 4, we shall conclude the present work.

## 2 Formalism

In this section, we describe the entire formalism required for our current study. In Sect. 2.1, we address the standard framework of the heavy quark potential in presence of an external magnetic field, and establish the connection with the gluon propagator through the dielectric permittivity. In the process, a temperature and magnetic field dependent Debye mass appears in the heavy quark potential through the gluon propagator. We calculate the Debye mass from semi-classical transport theory, whose thermomagnetic phase space can be obtained by projecting the temperature and magnetic field dependent condensates from the lattice quantum chromodynamics (LQCD) calculation. Through those medium dependent condensates we also incorporate the effects of both MC and IMC. This part is discussed in details in Sect. 2.2, which is the main motivation behind our present study. Next in Sect. 2.3 we discuss the framework of evaluating the thermal width and the binding energy for heavy quarkonia (e.g.  $J/\psi$  or  $\Upsilon$ ) from the imaginary and the real part of the heavy quark potential respectively.

### 2.1 In-medium heavy quark potential in presence of magnetic field

Let us start our discussion with the full Cornell potential [38, 46], that contains the Coulombic as well as the string part, given as,

$$V(r) = -\frac{\alpha}{r} + \sigma r. \quad (1)$$

Here,  $r$  is the relative position of the heavy quark and anti-quark,  $\alpha$  is the strong coupling constant given by ( $\alpha = \alpha_s C_F = \frac{g_s^2 C_F}{4\pi}$ ;  $C_F = 4/3$ ) and  $\sigma$  is the string tension. The Fourier transform of  $V(r)$  in the momentum space is obtained as

$$V(k) = -\sqrt{\frac{2}{\pi}} \left( \frac{\alpha}{k^2} + 2 \frac{\sigma}{k^4} \right). \quad (2)$$

It should be mentioned here that we have taken the spatially isotropic form of the heavy quark potential (see Eq. (1)) to obtain the in-medium modifications. In general the spacial form of the potential may have anisotropic structure due to the breaking of spherical symmetry in presence of magnetic field [47]. In our present work, the in-medium modifications have been obtained in the momentum space by dividing the vacuum heavy-quark potential with the medium dielectric permittivity  $\epsilon(\mathbf{k}, T, eB)$ , which carries the information of temperature and magnetic field. Hence the medium modified heavy quark potential in momentum space comes out to be,

$$\tilde{V}(k, T, eB) = \frac{V(k)}{\epsilon(k, T, eB)}, \quad (3)$$

which in turn gives (via the inverse Fourier transform)

$$\tilde{V}(r, T, eB) = \int \frac{d^3\mathbf{k}}{(2\pi)^{3/2}} (e^{i\mathbf{k}\cdot\mathbf{r}} - 1) \tilde{V}(k, T, eB). \tag{4}$$

In the above equation, perturbative free energy of infinite separated quarkonium contribution is subtracted through the  $r$ -independent term to renormalize the heavy quark free energy [48,49]. The medium dielectric permittivity  $\epsilon(k, T, eB)$  introduced for our purpose is connected with the longitudinal part of the gluon self energy [50]. Subsequently it can be obtained from the  $\omega \rightarrow 0$  limit of the temporal component of the medium dependent effective gluon propagator ( $\Delta^{00}$ ) as [1,50],

$$\epsilon^{-1}(\mathbf{k}, T, eB) = - \lim_{\omega \rightarrow 0} k^2 \Delta^{00}(\omega, \mathbf{k}, T, eB). \tag{5}$$

Now, to obtain respectively the real and the imaginary parts of the heavy quark potential in the static limit, the real and imaginary parts of the temporal component of the retarded propagator in the Fourier space is required [51], i.e.

$$\text{Re}[\Delta^{00}(\omega = 0, \mathbf{k}, T, eB)] = \frac{-1}{k^2 + m_D^2(T, eB)}, \tag{6}$$

$$\text{Im}[\Delta^{00}(\omega = 0, \mathbf{k}, T, eB)] = \pi T m_D^2 \tag{7}$$

$$\left\{ \frac{-1}{k\{k^2 + m_D^2(T, eB)\}^2} \right\}. \tag{8}$$

Finally we can further simplify the real and imaginary parts of the potential in terms of a modified coordinate space  $\hat{r} = rm_D$  by taking the short-distance limit  $\hat{r} \ll 1$  [45,52,53]. This yields following simplified expressions :

$$\text{Re } \tilde{V}(\hat{r}; T, B) = \left( \frac{2\sigma}{m_D} - \alpha m_D \right) \frac{e^{-\hat{r}}}{\hat{r}} - \frac{2\sigma}{m_D \hat{r}} + \frac{2\sigma}{m_D} - \alpha m_D, \tag{9}$$

$$\text{Im } \tilde{V}(\hat{r}; T, B) = T \left( \frac{\alpha \hat{r}^2}{3} - \frac{\sigma \hat{r}^4}{30 m_D^2} \right) \log \left( \frac{1}{\hat{r}} \right). \tag{10}$$

One can notice that with this simplification, the information of  $T$  and  $eB$  in the heavy quark potential are solely entering through the Debye mass  $m_D = m_D(T, B)$ , which we address in the next subsection.

### 2.2 Debye mass in presence of magnetic field

Debye screening mass is an important observable in the context of heavy ion collisions which also acts as a QGP signature through heavy quarkonia (i.e.  $J/\Psi$  and  $\Upsilon$ ) suppression. Debye screening mass can be directly evaluated from the temporal component of the gluon self energy tensor ( $\Pi_{00}(\omega, \mathbf{k})$ )

by employing the static limit ( $k = 0, \omega \rightarrow 0$ ) through a perturbative order by order evaluation. On the other hand one can also determine the Debye screening mass through the semi-classical transport theory by using the relation [45,54,55]

$$m_D^2 = g_s^2 C_{q/g} \int \frac{d^3k}{(2\pi)^3} \frac{d}{d\omega} f_{q/g}(\omega), \tag{11}$$

where  $g_s^2 \equiv 4\pi\alpha_s$  is the strong coupling constant,  $C_{q/g}$  are the Casimir constants for quarks and gluons and  $f_{q/g} = \frac{1}{e^{\beta\omega} \pm 1}$  are their respective distribution functions – Fermi-Dirac (FD) for quark and Bose-Einstein (BE) for gluons. For an ideal non interacting QGP medium, one can readily trace back the leading order hard thermal loop (HTL) expression of the Debye mass, i.e.  $m_D^2 = \frac{g_s^2 T^2}{3} (N_c + N_f/2)$ . There are several investigations on the Debye screening masses of the QGP as a function of the magnetic field from the temporal component of the gluon polarization tensor in perturbative QCD (pQCD) calculation [33,34,56–60], whose equivalent analogy in the semi-classical transport theory has been shown in Ref. [61]. The gluonic distribution function remains unchanged in presence of an external anisotropic magnetic field along the  $z$  direction ( $\mathbf{B} = B\hat{z}$ ), whereas the quark distribution function gets modified to:

$$f_q^l = \frac{1}{\exp(\beta E_f^l) + 1}, \tag{12}$$

where the Landau quantized dispersion relation reads as  $E_f^l = \sqrt{k_z^2 + m_f^2 + 2l|q_f eB|}$ , with  $l = 0, 1, 2, ..$  being the number of Landau levels and  $q_f = +\frac{2}{3}, -\frac{1}{3}$  being the fractional charge of the  $u$  and  $d$  quarks respectively. Again, in a magnetized medium the phase space quantization [62–64] can be represented as

$$\int \frac{d^3k}{(2\pi)^3} \rightarrow \frac{|q_f eB|}{2\pi} \sum_{l=0}^{\infty} \int \frac{dk_z}{2\pi} (2 - \delta_{0l}). \tag{13}$$

Incorporating these, the expression for the Debye screening mass  $m_D$  for a magnetized QGP medium becomes,

$$m_D^2 = g_s^2 T^2 \frac{N_c}{3} + \frac{g_s^2 |q_f eB|}{\pi^2 T} \int_0^{\infty} dk_z \sum_{l=0}^{\infty} (2 - \delta_{0l}) f_q^l (1 - f_q^l). \tag{14}$$

Now, in the earlier studies of the Debye screening mass in a magnetized medium [33,34,56–61], one important aspect has not been considered, namely the effect of IMC near the transition temperature. Taking this opportunity in the present work we have captured both the effects of MC and

IMC through the medium dependent constituent quark mass  $M_f(T, B)$  which is evaluated from the LQCD predicted values for the normalized quark condensates  $\langle q\bar{q} \rangle_f(T, eB)$  [12, 13]. The quark condensates in Refs. [12, 13] are normalized such a way that with increasing temperature it varies from 1 to 0 during the chiral phase transition at  $eB = 0$ , simultaneously bringing the quark mass down from  $M_f(T = 0)$  to bare mass  $m_f$ . Using this consequently at finite  $eB$  we can also build a connection between the medium dependent  $M_f(T, eB)$  and LQCD predicted condensates  $\langle q\bar{q} \rangle_f(T, eB)$  as

$$M_f(T, eB) = M_f(T = 0, eB = 0) \times \langle q\bar{q} \rangle_f(T, eB) + m_f \approx M_f(T = 0, eB = 0) \times \langle q\bar{q} \rangle_f(T, eB). \tag{15}$$

After fixing the effective constituent mass subsequently we redefine our dispersion relation in a magnetized medium as

$$\bar{E}_f^l = \sqrt{k_z^2 + 2l|q_f eB| + M_f(T, eB)^2}. \tag{16}$$

Using the LQCD data of  $\langle q\bar{q} \rangle_f(T, eB)$  from Ref. [12] in Eq. (15), we have plotted constituent quark mass  $M_{f=u,d}$  against  $T$  (upper panels) and  $eB$  (lower panels) in Fig. 1. Here, one can clearly notice that the constitute quark mass follow MC in low temperature domain and IMC near the transition temperature. Enhancement of the constituent quark mass with increasing values of  $eB$  in low  $T$  is noticed in the upper panels of Fig. 1 as well as in its lower panels (curves for  $T = 113$  MeV), mapping the MC effect of the quark condensates. On the other hand, reduction of the constituent quark mass with increasing values of  $eB$  near the transition temperature is also observed in Fig. 1. We notice that the constituent quark masses at  $T = 153$  MeV first increase and then subsequently decrease with increasing  $eB$ , clearly mapping the IMC effect of the quark condensates. Corresponding theoretical uncertainties originating from the LQCD extractions are also represented in Fig. 1 through various color bands.

With the Lattice QCD inspired modified dispersion relation from Eq. (16) we have finally evaluated the Debye screening mass as

$$m_D^2 = g_s^2(T)T^2 \frac{N_c}{3} + \sum_f \frac{g_s^2(T)|q_f eB|}{\pi^2 T} \times \int_0^\infty dk_z \sum_{l=0}^\infty (2 - \delta_{l0}) f_q^l(\bar{E}_f^l) (1 - f_q^l(\bar{E}_f^l)), \tag{17}$$

where we have considered  $g_s(T)$  – the temperature dependent one loop running coupling [65]:

$$g_s^2(T) = 4\pi\alpha_s(T) = \frac{24\pi^2}{(11N_c - 2N_f) \ln\left(\frac{2\pi T}{\Lambda_{\overline{MS}}}\right)}, \tag{18}$$

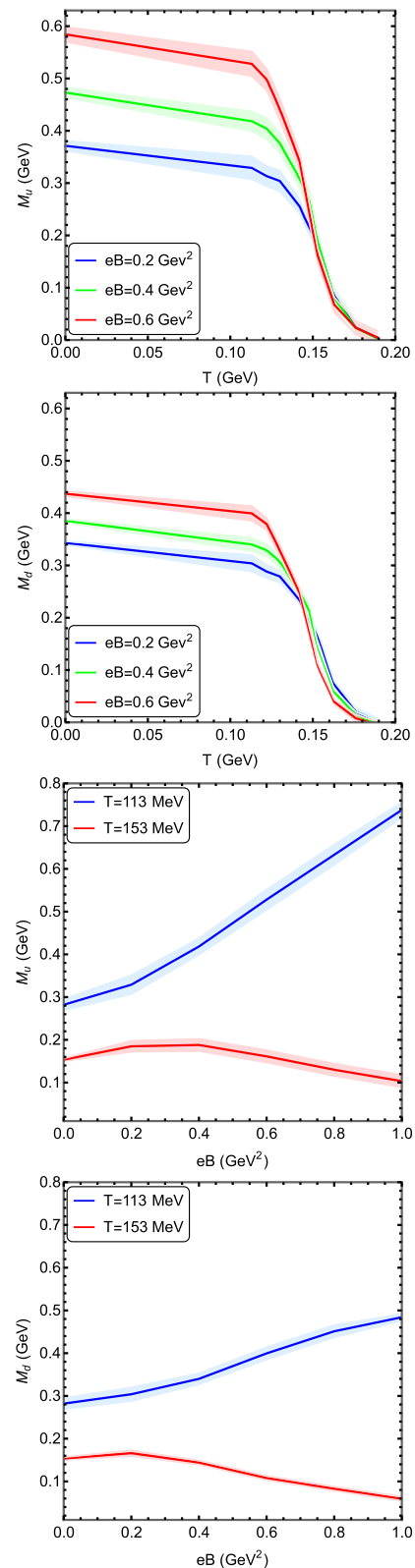


**Fig. 1** Variation of the constituent quark masses ( $M_u$  and  $M_d$ ) with temperature for different values of magnetic field  $eB = 0.2, 0.4, 0.6 \text{ GeV}^2$  in the upper panels and with magnetic field for different values of  $T = 113, 153 \text{ MeV}$  in the lower panels. The corresponding color bands represent the estimated theoretical uncertainties due to the LQCD extractions, which for the case of  $M_u/M_d$  is up to maximum  $\sim 10\%$

with  $\Lambda_{\overline{\text{MS}}}$  being the  $\overline{\text{MS}}$  renormalization scale.

### 2.3 Thermal width and binding energy

Next, we focus on other relevant quantities like thermal width or dissociation rate, binding energy in the context of heavy quark potential. Their working formulas are described below.

Let us first discuss about thermal width or dissociation rate  $\Gamma$ , which can be formulated from the imaginary part of potential  $\text{Im } \tilde{V}(r, T, B)$ , discussed in Sect. 2.1. Assuming that we know the  $r$ -profile of quarkonia wave function  $\Psi(r)$ , the thermal width  $\Gamma$  can be computed as [45]

$$\Gamma(T, B) = - \int d^3\mathbf{r} |\Psi(r)|^2 \text{Im } \tilde{V}(\hat{r}; T, B), \tag{19}$$

where imaginary part of the potential is folded by the unperturbed (1S) Coulomb wave function, owing to the first-order perturbation theory. Here we consider both  $\Psi_{1s}(r)$  and  $\Psi_{2s}(r)$  as Coulombic wave functions for the ground state ( $1s, J/\psi$  and  $\Upsilon$ ) and the first excited state ( $2s, \psi'$  and  $\Upsilon'$ ), respectively given as

$$\Psi_{1s}(r) = \frac{1}{\sqrt{\pi r_B^3}} e^{-\frac{r}{r_B}}, \tag{20}$$

$$\Psi_{2s}(r) = \frac{1}{2\sqrt{2\pi r_B^3}} \left( 2 - \frac{r}{r_B} \right) e^{-\frac{r}{2r_B}}, \tag{21}$$

where,  $r_B=2/(\alpha_s m_Q)$  is the Bohr radius of the quarkonia system with  $m_Q$  being the mass of the heavy quarks (charm ( $c$ )/bottom ( $b$ )) originating from different quarkonia states. We should mention here that the actual wave function in presence of an external magnetic field is more complicated in form and might be more challenging to solve. We know that the magnetic field in Schrodinger’s equation appears in the form of the harmonic oscillator potential, so one can expect a Hermite-like wave function for free particles [20]. Instead we have used a simple Coulomb type wave function following Refs. [33,35]. By solving Eq. (19), within the leading logarithmic order we obtain [45,68]

$$\Gamma_{1s}(T, B) = \left( 1 + \frac{3\sigma}{\alpha_s m_Q^2} \right) \frac{4T}{\alpha_s} \frac{m_D^2}{m_Q^2} \log \frac{\alpha_s m_Q}{2m_D}, \tag{22}$$

$$\Gamma_{2s}(T, B) = \left( 7 + \frac{192\sigma}{\alpha_s^3 m_Q^2} \right) \frac{8T}{\alpha_s} \frac{m_D^2}{m_Q^2} \log \frac{\alpha_s m_Q}{2m_D}, \tag{23}$$

Here also, one can see that the  $T$  and  $B$  dependent profile of  $\Gamma$  is coming through  $m_D(T, B)$ .

To obtain the binding energy, following Ref. [41], we consider a simple Coulombic type real part of heavy quark potential (where we take the short distance limit  $\hat{r} \ll 1$  and ignore

the  $\hat{r}$  independent terms by the virtue of translational invariance). By solving its corresponding Schrödinger equation, we can get the eigenvalues for charmonium and bottomonium system as

$$E_n = - \frac{1}{n^2} \frac{m_Q \sigma^2}{m_D^4}. \tag{24}$$

Now its ground state and first excited state eigen values for  $n = 1$  and  $n = 2$  respectively can be considered as binding energies of lowest and next to lowest possible charmonium/ bottomonium states, i.e.  $(J/\psi)/\Upsilon$  and  $\psi'/\Upsilon'$  respectively. Similar to thermal width  $\Gamma(T, B)$ , binding energies  $E_{n=1}(T, B)$  of  $J/\psi$  and  $\Upsilon$  and  $E_{n=2}(T, B)$  of  $\psi'$  and  $\Upsilon'$  will carry the magnetic field dependent information solely through the Debye mass  $m_D(T, B)$ .

### 3 Results

In this section we will show and discuss our results corresponding to heavy quark potential in a magnetized medium incorporating IMC based quark condensate. In the present work we have used  $N_c = 3, N_f = 2$  and  $\Lambda_{\overline{\text{MS}}} = 0.176 \text{ GeV}$  [66], the string tension,  $\sigma = 0.184 \text{ GeV}^2$  [68] and the value of  $\alpha_s$  from Eq. (18).

In the formalism part, we have already discussed about the Fig. 1, which graphically represent the  $T$  and  $eB$  profiles of the constituent quark mass, based on the LQCD inspired quark condensates. Hence here we start with the Debye mass which carries the MC and IMC profiles through the medium dependent constituent quark mass. Before discussing the plots though, we want to mention about the theoretical uncertainties. We have previously reported that the theoretical uncertainties corresponding to the constituent quark masses is up to maximum  $\sim 10\%$ , which we represented in Fig. 1 through various color bands. Proceeding further, when we plug that uncertainty in the expression for the Debye mass, it gets exponentially suppressed and turns out to be really small, i.e. maximum  $\sim 0.02\%$ . Hence for the remainder of our results we have neglected these LQCD-based uncertainties. In the left panel of Fig. 2, we have plotted the variation of the Debye mass with  $T$  for different values of magnetic fields, i.e.  $eB = 0.2$  (black solid line),  $0.4$  (dashed line),  $0.6$  (dotted line)  $\text{GeV}^2$ . Whereas, the right panel of the Fig. 2 shows the variation of the Debye mass with  $eB$  for different values of temperature, i.e.  $T = 100$  (solid line), and  $200$  (dashed line)  $\text{MeV}$ . If we follow the Debye screening mass expression, given in Eq. (17), then we can identify the  $T$  and  $eB$  dependent mathematical components. Sources of  $T$  are the FD distribution function  $f_q^l(T)$  and coupling constant  $g_s(T)$ , which provide increasing and decreasing  $T$  profiles. Hence, due to their collective roles, we notice that  $m_D(T)$  decreases first and then starts increasing. On the other



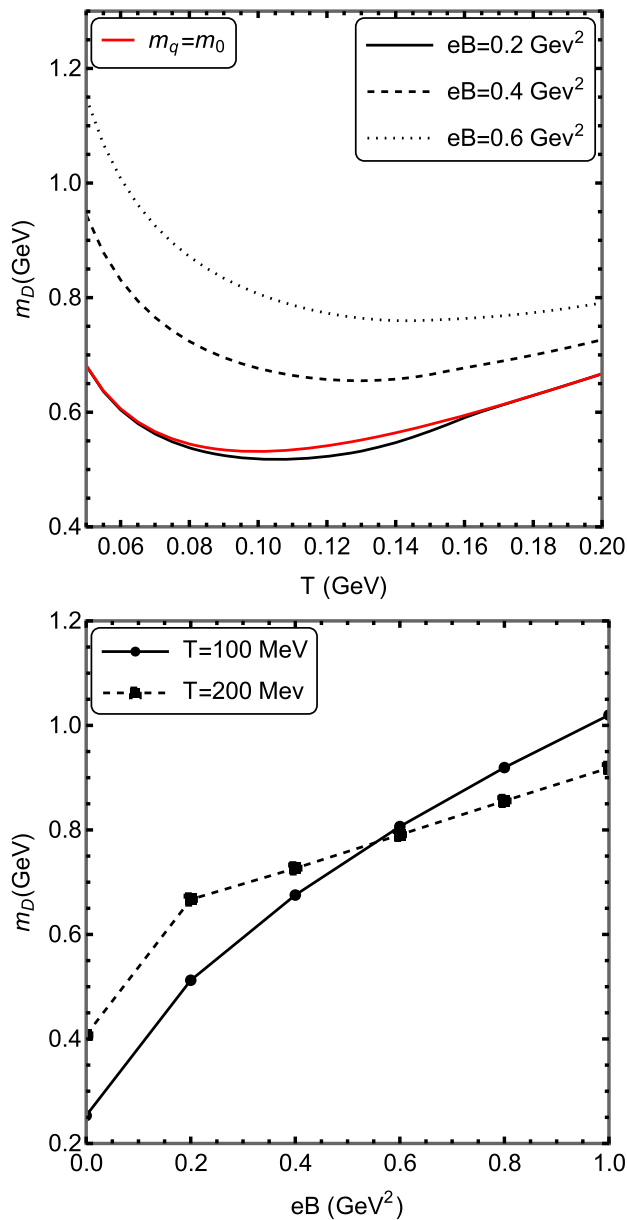


**Fig. 2** Variation of the Debye mass ( $m_D$ ) with temperature for different values of magnetic fields  $eB = 0.2$  (black solid line),  $0.4$  (dash line),  $0.6$  (dotted line)  $\text{GeV}^2$  in left panel and with magnetic field for different values of temperatures  $T = 100$  (black solid line),  $200$  (dash line)  $\text{MeV}$  in right panel. Red solid line in left panel denotes for massless quark case

hand, regarding the  $eB$  dependence of the Debye mass one can notice a straight forward  $m_D \propto eB$  relation in Eq. 17. However, right panel of Fig. 2 shows deviations from the proportional relation, which is because of a non-trivial  $eB$  dependence entering through the  $eB$  dependent constituent quark mass  $M_f(T, eB)$ , located in FD distribution function. Also we notice that the effect of magnetic field is stronger at a lower temperature and becomes weaker at a higher temperature.

Now, if we compare our results with earlier  $m_D(T, eB)$  calculations, done in Refs. [33,34,56–61], then one can find that the new aspect of present work is the adoption of IMC based constituent quark mass. Quark condensate and constituent quark mass are the usual quantities, where one can clearly observe the IMC effect near the transition temperature. On the other hand, for an important observable like Debye mass  $m_D(T, eB)$ , it is usually not zoomed in as it becomes fade due to the integration of thermal distributions. For thermodynamical quantities like pressure, energy density or transport coefficients like electrical conductivity [67], we get similar results. Emphasising this point here, we will continue to present our final results as an IMC based outcome instead of zooming in the actual modification, which is quite mild in graphical representation. To explicitly point out this modification in the left panel of Fig. 2, we have also plotted the Debye mass considering massless quark case (red solid line) for  $eB = 0.2 \text{ GeV}^2$  and compared it with black solid line, which has considered IMC based constituent quark mass  $M_f(T, eB)$ . Within the range of  $T = 0.080\text{-}0.160 \text{ GeV}$ , a mild suppression of Debye mass is noticed for the IMC based constituent quark mass  $M_f(T, eB)$  in place of the current quark mass. This suppression of Debye mass is connected with the magnetized quark condensate in non-perturbative QCD (non-pQCD) domain, obtained from LQCD calculation [12,13], which reveals the IMC effect near transition temperature. So, this effect will propagate to other quantities of heavy quark phenomenology, as we discuss next.

In Fig. 3 we have plotted the variation of the real part of the potential with the separation distance ( $r$ ) between the  $Q\bar{Q}$  pair for different values of magnetic field ( $eB = 0, 0.2 \text{ GeV}^2$  and  $0.4 \text{ GeV}^2$ ) and at two different values of temperature, i.e.  $T = 100 \text{ MeV}$  (left panel) and  $T = 200 \text{ MeV}$  (right panel). From Fig. 3 we find that the screening is increasing with the increase in magnetic field and temperature. One can notice that the exponential decay with distance becomes more at a higher temperature ( $T = 200 \text{ MeV}$  in right panel) as compared to lower temperature ( $T = 100 \text{ MeV}$  in left panel). By shifting from zero to non-zero magnetic field and increasing its values, similar dominance in the exponential behavior is noticed. It is because the exponential decay term is controlled by the Debye mass, which increases with  $T$  as well as  $eB$ . Hence this enhancement of the screening with  $T$  and  $eB$  indicates loosely bound quarkonium states at high  $T$  and  $eB$ .

Similar to the real-part of the potential, in Fig. 4 we have plotted the imaginary part of the potential with the separation distance ( $r$ ) for different values of magnetic field ( $eB = 0, 0.2 \text{ GeV}^2$  and  $0.4 \text{ GeV}^2$ ) at  $T = 100 \text{ MeV}$  (left panel) and  $T = 200 \text{ MeV}$  (right panel). As we can see from the figure that magnitude of the imaginary part of the potential increases with the increase in magnetic field and hence it provides more contribution to the thermal width obtained

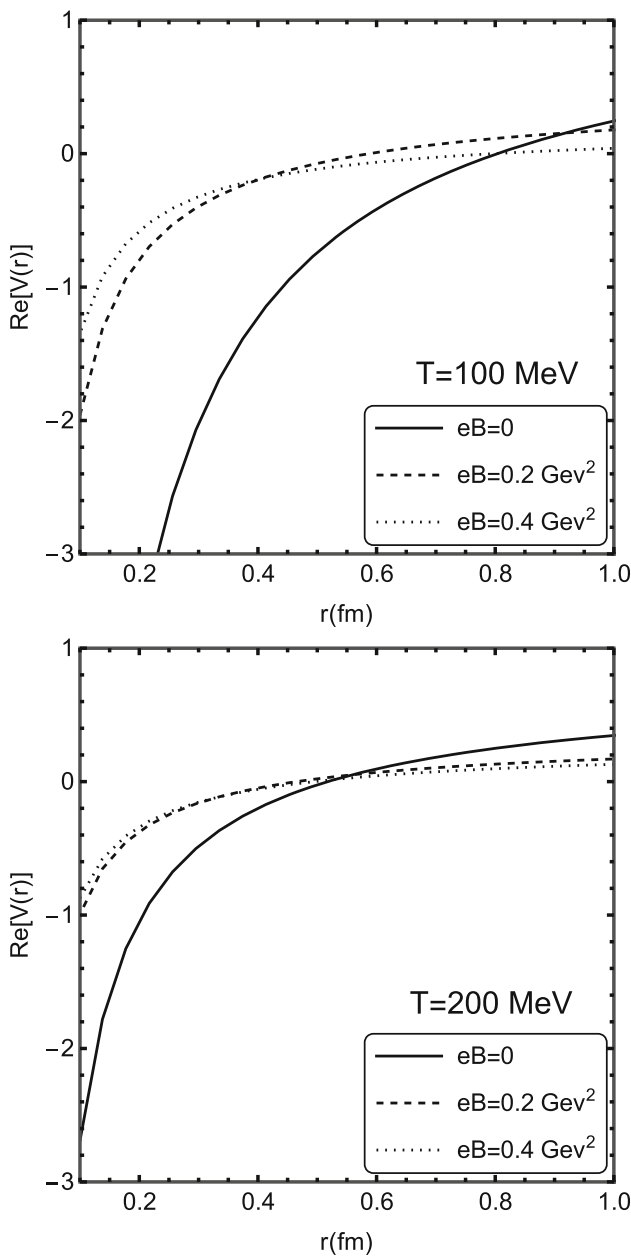


**Fig. 3** Variation of the real part of potential with separation distance  $r$  between  $Q\bar{Q}$  for three different values of the magnetic field and with fixed temperature  $T = 100$  MeV (left) and  $T = 200$  MeV (right)

from the imaginary part of the potential. We also find that the magnitude of imaginary part of potential is more at a higher temperature ( $T = 200$  MeV) as compared to a lower temperature ( $T = 100$  MeV) for a given  $eB$  and  $r$ . This behaviour is again due to the aforementioned  $T$  and  $eB$  dependence of the Debye mass. So, grossly we notice that real and imaginary parts of heavy quark potential are modified with  $T$  and  $eB$  due to the non-trivial profile of LQCD based quark condensates and these modifications suggest towards more screening and dissociation with increasing of  $T$  and  $eB$ . They also indicate

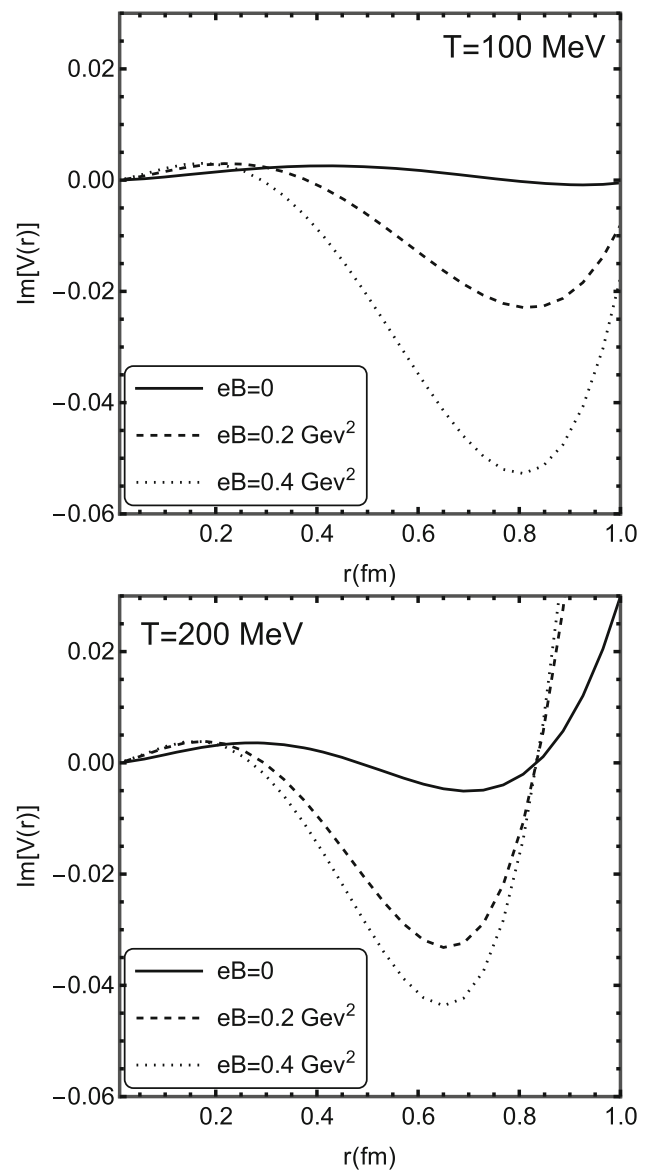


**Fig. 4** Variation of the imaginary part of potential with separation distance  $r$  between  $Q\bar{Q}$  for various values of magnetic field  $T = 100$  MeV (left) and  $T = 200$  MeV (right)

the possibilities of low dissociation temperatures due to the external magnetic field, which we will explicitly see later.

Next, let us integrate out the separation distance  $r$  dependence of imaginary and real potential through Coulomb-type probability distribution functions and proceed to compute respectively the thermal width or dissociation probability  $\Gamma(T, B)$  by using Eqs. (22)/(23) and binding energy using the Eq. (24). Imaginary and real part of the heavy quark potential are their respective sources, whose  $T$  and  $eB$  profiles are mainly coming from the modified medium dependent Debye mass  $m_D(T, eB)$ .

Let us first discuss about binding energy (BE), plotted in Fig. 5. The left panel of Fig. 5 shows the binding energies

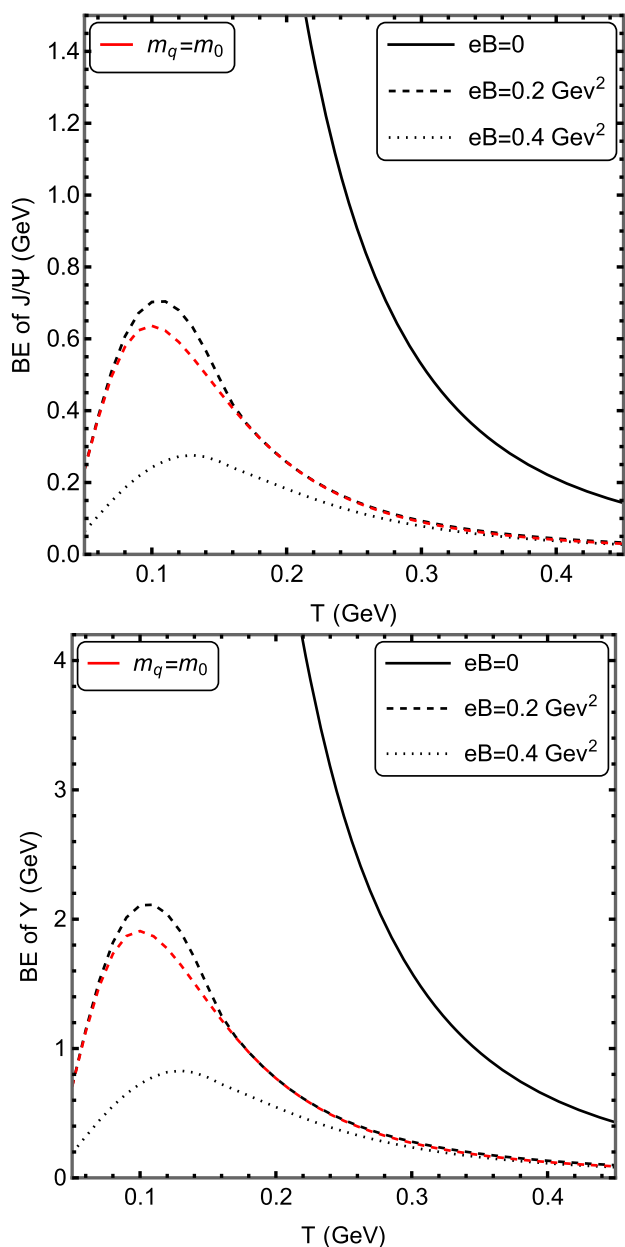


**Fig. 5** Variation of binding energy (in GeV) with temperature with different values of magnetic field ( $eB$ ) for  $J/\psi$  (left panel) and  $\Upsilon$  (right panel)

of  $J/\psi$  as a function of  $T$  for various values of magnetic field, i.e.  $eB = 0$  (solid line),  $0.2$  (dashed line) and  $0.4 \text{ GeV}^2$  (dotted line). For the purpose of comparison we have also showed the result considering current quark mass for  $eB = 0.2 \text{ GeV}^2$  (red dashed line). We observe that binding energy is decreasing as the temperature and magnetic field both are increasing. In the right panel of Fig. 5 we show an exactly similar plot for the binding energies of  $\Upsilon$  as a function of  $T$ . The similar behaviour has been observed for  $\Upsilon$  also, except that the value of binding energy for  $J/\psi$  is lower as compared to the value for  $\Upsilon$ , which is due to their mass difference.

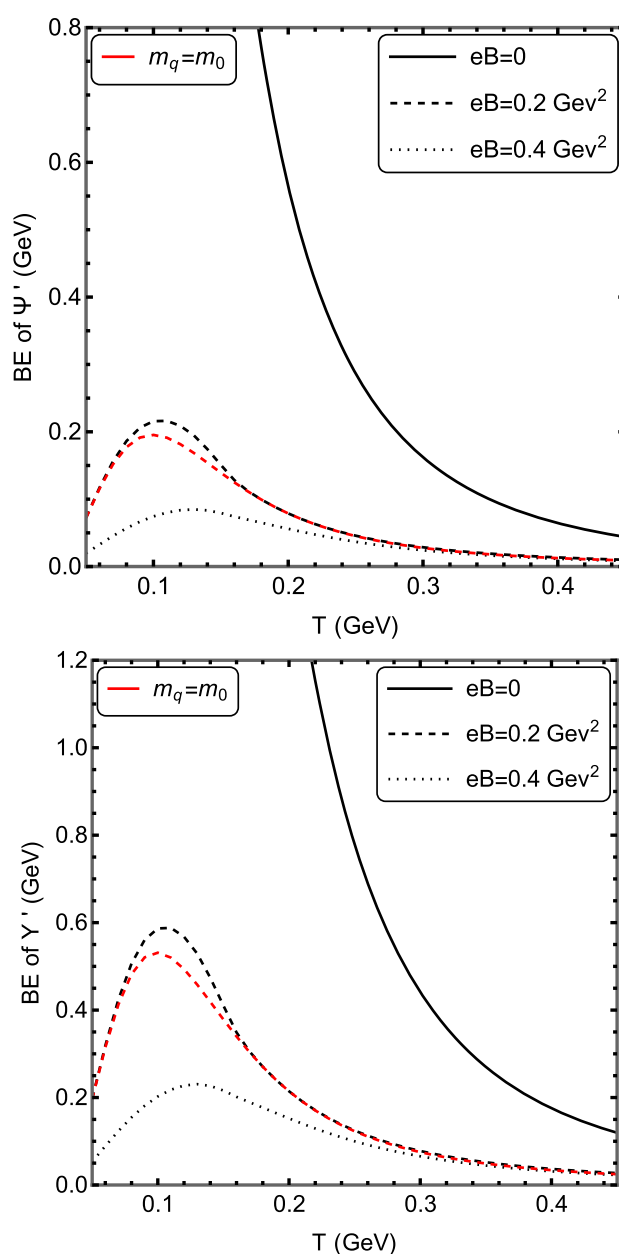


**Fig. 6** Variation of binding energy (in GeV) with temperature with different values of magnetic field ( $eB$ ) for  $\psi'$  (left panel) and  $\Upsilon'$  (right panel)

In Fig. 6 we have also presented the binding energies of  $\psi'$  in the left panel and  $\Upsilon'$  in the right panel as a function of  $T$ . While comparing the binding energies of  $J/\psi$  and  $\psi'$ , we notice that the binding energy is less for the  $\psi'$  case as compared to  $J/\psi$ . This implies that the former will dissolve after the latter one. Similar statement could be made for  $\Upsilon$  and  $\Upsilon'$ . We want to note at this point that for our purpose, we have taken (charmonium)  $J/\psi$ , (bottomonium)  $\Upsilon$ , (psi prime)  $\psi'$ , and (upsilon prime)  $\Upsilon'$  masses as  $m_c = 3.096 \text{ GeV}$ ,  $m_b = 9.460 \text{ GeV}$ ,  $m_{\psi'} = 3.686 \text{ GeV}$  and  $m_{\Upsilon'} = 10.023 \text{ GeV}$  respectively.



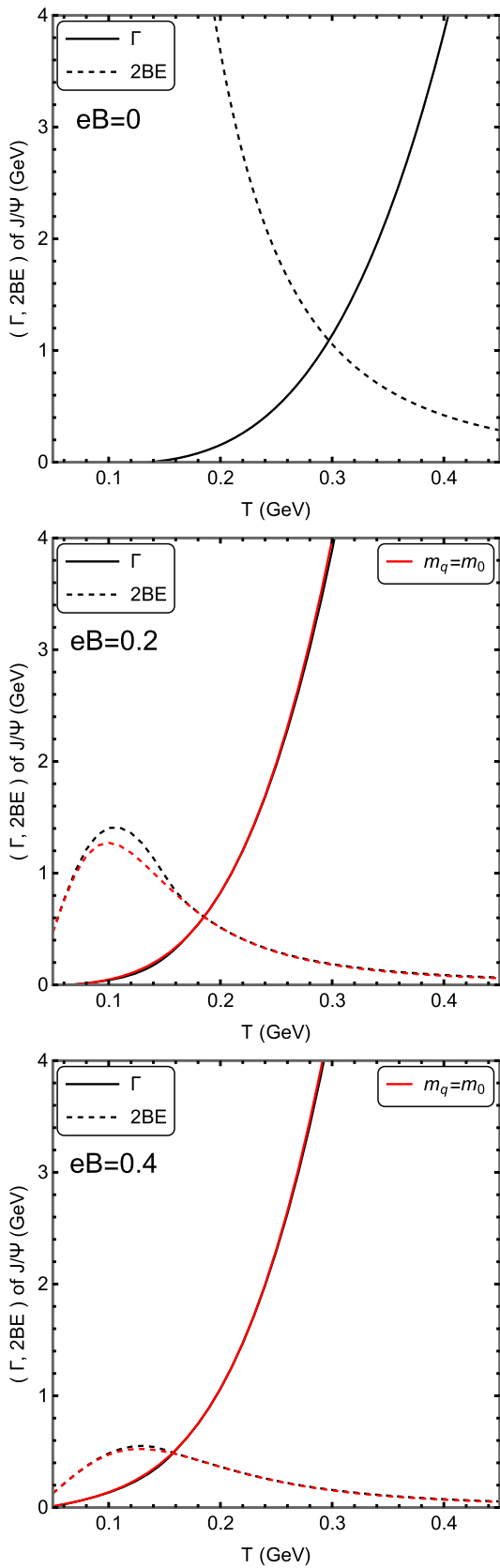


**Fig. 7** Variation of  $\Gamma$ , 2BE with temperature with different values of magnetic field (eB) for  $J/\psi$

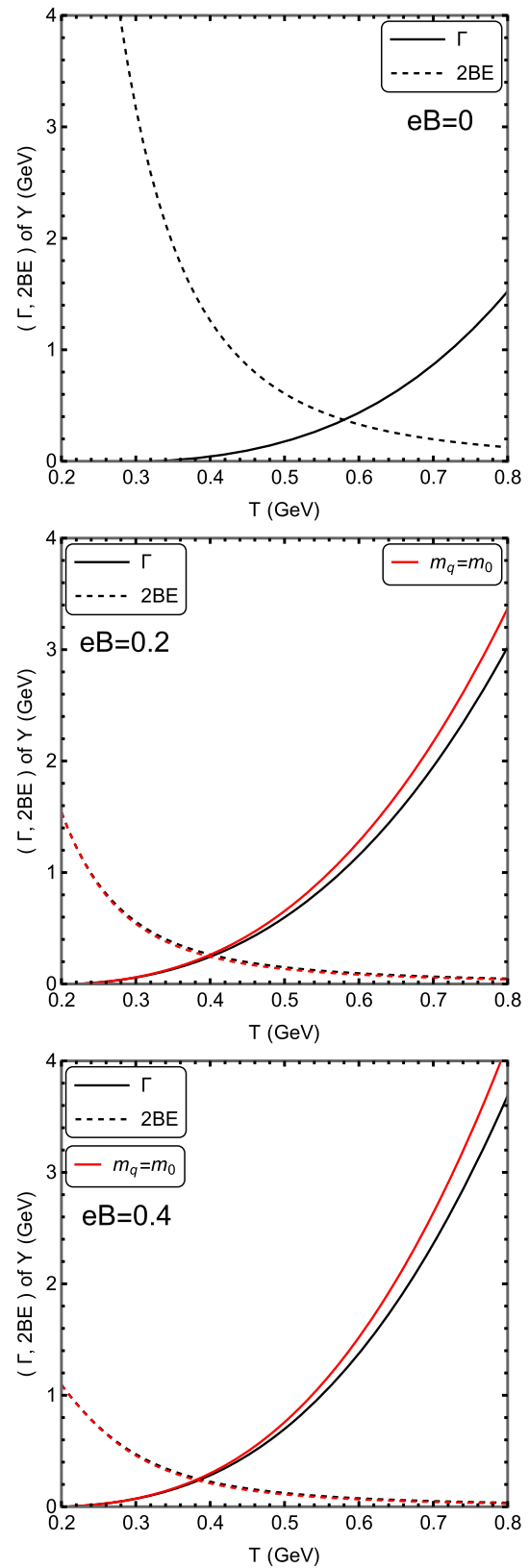


**Fig. 8** Variation of  $\Gamma$ , 2BE with temperature with different values of magnetic field (eB) for  $\Upsilon$

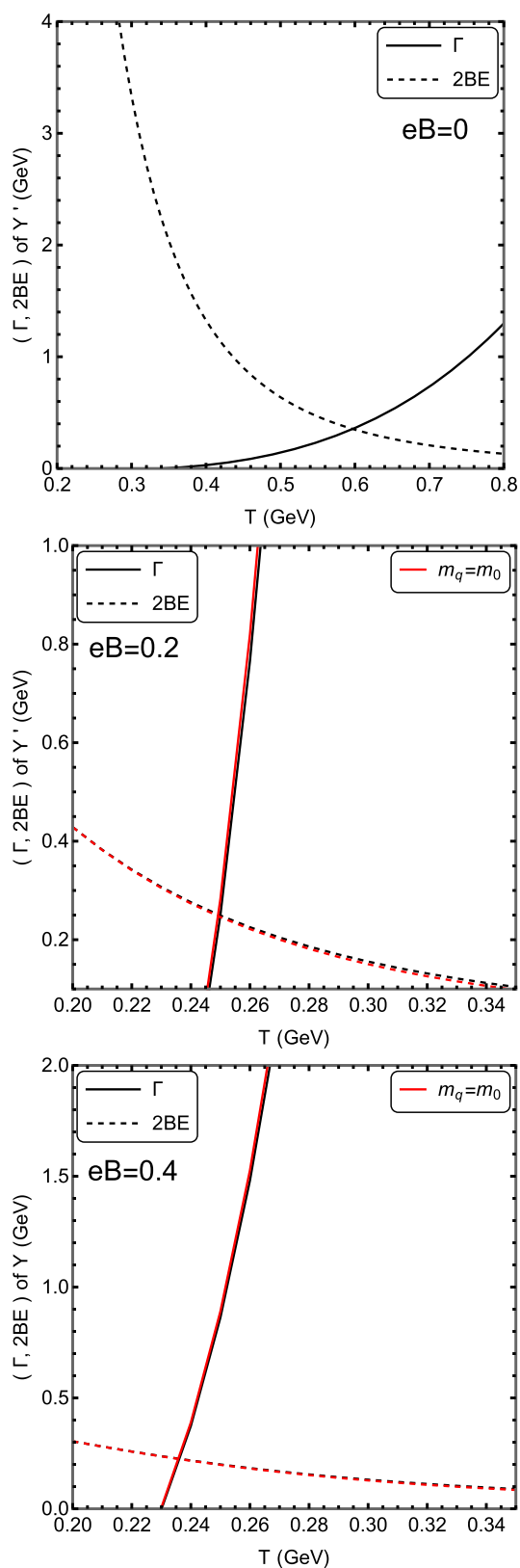


**Fig. 9** Variation of  $\Gamma$ ,  $2BE$  with temperature with different values of magnetic field ( $eB$ ) for  $\Upsilon'$

Further we estimate the thermal width or dissociation probability, given in Eqs. (22)/(23), which is obtained by substituting Eq. (10) in Eq. (19). In other words Eq. (10) represents a detailed tomography of dissociations of quarkonia state, while Eq. ((19)) present its integrated values. Now this heavy quark bound states (quarkonia) can be dissociated completely when thermal width becomes greater than twice of the the binding energy i.e.  $\Gamma \geq 2BE$  [69]. Hence, if one simultaneously plots twice the binding energy ( $2BE$ ) and the thermal width ( $\Gamma$ ) against  $T$ , then their intersection point can be considered as dissociation temperature ( $T_d$ ). We have plotted this in Figs. 7, 8 and in 9 for ground state of charmonium ( $J/\psi$ ), bottomonium ( $\Upsilon$ ) and upsilonprime ( $\Upsilon'$ ) respectively with three different values of magnetic field, i.e.  $eB = 0$  (left panel),  $eB = 0.2 \text{ GeV}^2$  (middle panel) and  $eB = 0.4 \text{ GeV}^2$  (right panel). There is no intersection point above the critical temperature ( $T_c$ ) for  $\psi'$ . This nature is expected because the excited states decay at low temperature than their corresponding ground state ( $J/\psi$ ).

If we further analyse Figs. 7, 8 and 9 we can observe that the thermal width is increasing with increasing magnetic field. Also we observe that the width for the  $J/\psi$  is much larger than that of the  $\Upsilon$ , because charmonium states are larger in size and smaller in masses as compared to bottomonium states which are smaller in size and larger in masses and hence will get dissociated at higher temperatures. On the otherhand, the excited state  $\Upsilon'$  has the lowest width. Interestingly, we notice the pattern of increasing  $\Gamma$  and decreasing  $BE$  with increasing magnetic field, which results in quicker dissociations of the quarkonium states. Our findings of the dissociation temperatures from the intersection points in Figs. 7, 8 and 9 are enlisted in Table 1. One can observe that the dissociation temperature is lowest for the excited state  $\Upsilon'$ . We notice that dissociation temperature of quarkonia states decreases as magnetic field increases. This fact is exactly similar with the reduction of the transition temperature due to magnetic field, which is connected with the IMC effect. If QCD follow MC near transition temperature, then magnetic field will push the location of transition temperature towards the higher values. However, reduction of dissociation temperature with magnetic field can not solely be linked with IMC as constituent quark mass has very mild impact on the Debye mass and heavy quark phenomenology. In other words, the fact of reduction of dissociation temperature with increasing magnetic field remains the same for both MC and IMC. This conclusion can be established from Figs. 7, 8 and 9, where we notice that the intersection point (vis-a-vis  $T_d$ ) remain almost same for IMC-based constituent quark mass (black line) and massless quark case (red line).

**Table 1** The dissociation temperature ( $T_D$ ) for the quarkonia states (in units of MeV), when  $\Gamma = 2BE$ 

State	$eB = 0$	$eB = 0.2$	$eB = 0.4$
$J/\psi$	297	186	158
$\Upsilon$	580	403	388
$\Upsilon'$	600	250	235

## 4 Conclusions

We have revisited the medium modified heavy quark potential at finite magnetic field. This is done by obtaining the real and imaginary parts of the resummed gluon propagator, which in turn gives the real and imaginary parts of the dielectric permittivity. In the process, a temperature and magnetic field dependent Debye mass enters into the gluon propagator where we have captured the essence of the inverse magnetic catalysis (IMC) through LQCD inspired quark condensates. Further we have used the real and imaginary parts of the dielectric permittivity to evaluate the real and imaginary parts of the complex heavy quark potential. We have noticed that the Debye screening mass increases with temperature and magnetic field, hence making the exponential term in the real part of potential more dominant. This in turn interprets more screening and favors the dissociation process. With respect to earlier works, present work has incorporated two new ingredients – inverse magnetic catalysis information and all Landau level summations within the Debye mass.

The real part of the potential is then used in the time-independent Schrödinger equation for the radial wave function to obtain the binding energy of heavy quarkonia, whereas the imaginary part is used to calculate the thermal width. We have observed the decreasing nature of the binding energies and increasing nature of the thermal widths of  $J/\psi$ ,  $\Upsilon$  and  $\Upsilon'$  with increasing values of the temperatures and magnetic fields. These behaviours of the binding energies and thermal widths of heavy quarkonia push its dissociation probability. So finally by plotting the twice of binding energy along with the thermal width, we have obtained the dissociation temperature as a point of their intersection. As our final observation we have noticed that the dissociation temperature of heavy quarkonia gets reduced due to the presence of the magnetic field, which can not be solely linked with the novel IMC effect incorporated in this work.

**Acknowledgements** IN, AB and RG acknowledges IIT Bhilai for the academic visit and hospitality during the course of this work. Authors are thankful to Mujeeb Hassan for useful discussion. I.N., A.B., R.G thank to Shivani Valecha, Sunima Baral, Srikanta Debata, Purushottam Sahu, Naba Kumar Rana for helping them in arranging accommodation. IN acknowledges the Women Scientist Scheme A (WoS A) of the Department of Science and Technology (DST) for the funding with grant no. DST/WoS-A/PM-79/2021. AB is supported by the

Guangdong Major Project of Basic and Applied Basic Research No. 2020B0301030008, Science and Technology Program of Guangzhou Project No. 2019050001 and the postdoctoral research fellowship from the Alexander von Humboldt Foundation, Germany. RG is funded by University Grants Commission (UGC).

**Data Availability Statement** This manuscript has no associated data or the data will not be deposited. [Authors' comment: We have not used any associated data in this article. We used Mathematica to produce the graphs.]

**Open Access** This article is licensed under a Creative Commons Attribution 4.0 International License, which permits use, sharing, adaptation, distribution and reproduction in any medium or format, as long as you give appropriate credit to the original author(s) and the source, provide a link to the Creative Commons licence, and indicate if changes were made. The images or other third party material in this article are included in the article's Creative Commons licence, unless indicated otherwise in a credit line to the material. If material is not included in the article's Creative Commons licence and your intended use is not permitted by statutory regulation or exceeds the permitted use, you will need to obtain permission directly from the copyright holder. To view a copy of this licence, visit <http://creativecommons.org/licenses/by/4.0/>.

Funded by SCOAP<sup>3</sup>. SCOAP<sup>3</sup> supports the goals of the International Year of Basic Sciences for Sustainable Development.

## References

1. H.A. Weldon, Phys. Rev. D **26**, 1394 (1982). <https://doi.org/10.1103/PhysRevD.26.1394>
2. E. Braaten, R.D. Pisarski, Nucl. Phys. B **337**, 569–634 (2019)
3. E. Braaten, R.D. Pisarski, Phys. Rev. D **45**(6), R1827 (1992)
4. J. Frenkel, J.C. Taylor, Nucl. Phys. B **334**, 199–216 (1990)
5. D.E. Kharzeev, L.D. McLerran, H.J. Warringa, Nucl. Phys. A **803**, 227 (2008)
6. V. Skokov, A.Y. Illarionov, V. Toneev, Int. J. Mod. Phys. A **24**, 5925 (2009)
7. L. McLerran, V. Skokov, Nucl. Phys. A **929**, 184 (2014)
8. K. Tuchin, Phys. Rev. C **83**, 017901 (2011)
9. A. Das, S.S. Dave, P.S. Saumia, A.M. Srivastava, Phys. Rev. C **96**(3), 034902 (2017)
10. T. Vachaspati, Phys. Lett. B **265**, 258 (1991)
11. D. Grasso, H.R. Rubinstein, Phys. Rep. **348**, 163 (2001)
12. G.S. Bali et al., QCD quark condensate in external magnetic fields. Phys. Rev. D **86**, 071502 (2012)
13. G.S. Bali et al., The QCD equation of state in background magnetic fields. J. High Energy Phys. **08**, 177 (2014)
14. L. McLerran, Rev. Mod. Phys. **58**, 1021 (1986)
15. B.B. Back et al. [PHOBOS], Nucl. Phys. A **757**, 28–101 (2005)
16. J.E. Augustin et al. [SLAC-SP-017], Phys. Rev. Lett. **33**, 1406–1408 (1974)
17. J.J. Aubert et al. [E598], Phys. Rev. Lett. **33**, 1404–1406 (1974)
18. F. Karsch, M.T. Mehr, H. Satz, Color screening and deconfinement for bound states of heavy quarks. Z. Phys. C **37**, 617 (1988)
19. T. Matsui, H. Satz, Phys. Lett. B **178**, 416 (1986)
20. J. Alford, M. Strickland, Phys. Rev. D **88**, 105017 (2013)
21. K. Marasinghe, K. Tuchin, Phys. Rev. C **84**, 044908 (2011)
22. S. Cho, K. Hattori, S.H. Lee, K. Morita, S. Ozaki, Phys. Rev. Lett. **113**(17), 172301 (2014)
23. X. Guo, S. Shi, N. Xu, Z. Xu, P. Zhuang, Phys. Lett. B **751**, 215 (2015)
24. C. Bonati, M. D'Elia, A. Rucci, Phys. Rev. D **92**(5), 054014 (2015)

25. R. Rougemont, R. Critelli, J. Noronha, *Phys. Rev. D* **91**(6), 066001 (2015)
26. D. Dudal, T.G. Mertens, *Phys. Rev. D* **91**, 086002 (2015)
27. A.V. Sadofyev, Y. Yin, *JHEP* **1601**, 052 (2016)
28. C.S. Machado, F.S. Navarra, E.G. de Oliveira, J. Noronha, M. Strickland, *Phys. Rev. D* **88**, 034009 (2013)
29. C.S. Machado, S.I. Finazzo, R.D. Matheus, J. Noronha, *Phys. Rev. D* **89**(7), 074027 (2014)
30. P. Gubler, K. Hattori, S.H. Lee, M. Oka, S. Ozaki, K. Suzuki, *Phys. Rev. D* **93**(5), 054026 (2016)
31. K. Fukushima, K. Hattori, H.U. Yee, Y. Yin, *Phys. Rev. D* **93**(7), 074028 (2016)
32. S.K. Das, S. Plumari, S. Chatterjee, J. Alam, F. Scardina, V. Greco, *Phys. Lett. B* **768**, 260 (2017)
33. B. Singh, L. Thakur, H. Mishra, *Phys. Rev. D* **97**(9), 096011 (2018)
34. M. Kurian, S. Mitra, S. Ghosh, V. Chandra, *Eur. Phys. J. C Part. Fields* **79**(2) (2019)
35. M. Hasan, B. Chatterjee, B.K. Patra, *Eur. Phys. J. C* **77**, 767 (2017)
36. A. Bandyopadhyay, J. Liao, H. Xing, [arXiv:2105.02167](https://arxiv.org/abs/2105.02167) [hep-ph]
37. W. Lucha, F.F. Schoberl, D. Gromes, *Phys. Rep.* **200**, 127 (1991)
38. E. Eichten, K. Gottfried, T. Kinoshita, K.D. Lane, T.M. Yan, *Phys. Rev. D* **21**, 203 (1980)
39. N. Brambilla, A. Pineda, J. Soto, A. Vairo, *Rev. Mod. Phys.* **77**, 1423 (2005)
40. E. Eichten, K. Gottfried, T. Kinoshita, J.B. Kogut, K.D. Lane, T. Yan, *Phys. Rev. Lett.* **34**, 369 (1975) [Erratum: *Phys. Rev. Lett.* **36**, 1276 (1976)]
41. V. Agotiya, V. Chandra, B.K. Patra, *Phys. Rev. C* **80**, 025210 (2009)
42. L. Thakur, N. Haque, U. Kakade, B.K. Patra, *Phys. Rev. D* **88**, 054022 (2013)
43. L. Thakur, U. Kakade, B.K. Patra, *Phys. Rev. D* **89**, 094020 (2014)
44. U. Kakade, B.K. Patra, L. Thakur, *Int. J. Mod. Phys. A* **30**(09), 1550043 (2015)
45. V.K. Agotiya, V. Chandra, M.Y. Jamal, I. Nilima, *Phys. Rev. D* **94**(9), 094006 (2016)
46. E. Eichten, K. Gottfried, T. Kinoshita, K.D. Lane, T.M. Yan, *Phys. Rev. D* **17**, 3090 (1978) [Erratum: *Phys. Rev. D* **21**, 313 (1980)]
47. S. Iwasaki, M. Oka, K. Suzuki, *Eur. Phys. J. A* **57**(7), 222 (2021). <https://doi.org/10.1140/epja/s10050-021-00533-5>. [arXiv:2104.13990](https://arxiv.org/abs/2104.13990) [hep-ph]
48. A. Dumitru, Y. Guo, M. Strickland, *Phys. Rev. D* **79**, 114003 (2009)
49. L. Thakur, U. Kakade, B.K. Patra, *Phys. Rev. D* **89**(9), 094020 (2014)
50. R.A. Schneider, *Phys. Rev. D* **66**, 036003 (2002)
51. Y. Burnier, M. Laine, M. Vepsäläinen, *Phys. Lett. B* **678**, 86 (2009)
52. V. Chandra, A. Ranjan, V. Ravishankar, *Eur. Phys. J. A* **40**, 109 (2009)
53. V. Agotiya, L. Devi, U. Kakade, B.K. Patra, *Int. J. Mod. Phys. A*, 1250009 (2012)
54. V. Chandra, V. Ravishankar, *Nucl. Phys. A* **848**, 330 (2010)
55. M.E. Carrington, A. Rebhan, *Phys. Rev. D* **79**, 025018 (2009)
56. S. Mitra, V. Chandra, *Phys. Rev. D* **96**(9), 094003 (2017)
57. A. Bandyopadhyay, C.A. Islam, M.G. Mustafa, *Phys. Rev. D* **94**(11), 114034 (2016)
58. B. Karmakar, R. Ghosh, A. Bandyopadhyay, N. Haque, M.G. Mustafa, *Phys. Rev. D* **99**(9), 094002 (2019)
59. C. Bonati, M. D'Elia, M. Mariti, M. Mesiti, F. Negro, A. Rucci, F. Sanfilippo, *Phys. Rev. D* **95**(7), 074515 (2017)
60. M. Kurian, V. Chandra, *Phys. Rev. D* **96**(11), 114026 (2017)
61. S. Ghosh, V. Chandra, Electromagnetic spectral function and dilepton rate in a hot magnetized QCD medium., *Phys. Rev. D* **98**(7), 076006 (2018)
62. A.N. Tawfik, *J. Phys. Conf. Ser.* **668**(1), 012082 (2016)
63. V.P. Gusynin, V.A. Miransky, I.A. Shovkovy, *Nucl. Phys. B* **462**, 249 (1996)
64. F. Bruckmann, G. Endrodi, M. Giordano, S.D. Katz, T.G. Kovacs, F. Pittler, J. Wellenhofer, *Phys. Rev. D* **96**(7), 074506 (2017)
65. N. Haque, *Phys. Rev. D* **98**(1), 014013 (2018). <https://doi.org/10.1103/PhysRevD.98.014013>. [arXiv:1804.04996](https://arxiv.org/abs/1804.04996) [hep-ph]
66. N. Haque, A. Bandyopadhyay, J.O. Andersen, M.G. Mustafa, M. Strickland, N. Su, *JHEP* **1405**, 027 (2014)
67. A. Bandyopadhyay, S. Ghosh, R.L.S. Farias, J. Dey, G. Krein, *Phys. Rev. D* **102**, 114015 (2020)
68. M.Y. Jamal, I. Nilima, V. Chandra, V.K. Agotiya, *Phys. Rev. D* **97**, 094033 (2018)
69. L. Thakur, U. Kakade, B.K. Patra, *Phys. Rev. D* **89**, 094020 (2014)